

# Properties and anti-biofouling activity of novel hybrid monophasic Cellulose Acetate/Silica/Titania membranes



Peixoto, Inês Parrinha

October 2019

## Abstract

Two series of novel monophasic integral asymmetric Cellulose Acetate/Silica/Titania (CA/SiO<sub>2</sub>/TiO<sub>2</sub>) (series 1) and Cellulose Acetate/Titania CA/TiO<sub>2</sub> (series 2) membranes with TiO<sub>2</sub> contents between 0 and 5wt.% were synthesized by the combination of phase inversion and sol-gel techniques. The membranes were characterized in terms of chemical structure, surface and cross-section morphology, permeation performance, bactericide potential and anti-biofouling properties.

Scanning Electron Microscopy revealed that all membranes present asymmetric cross-section structures characterized by a very thin (<1µm) dense active layer and a thicker porous substructure. Fourier Transform Infra-Red and Inductively Coupled Plasma Optical Emission Spectrometry revealed that TiO<sub>2</sub> is covalently bonded to CA and homogeneously distributed throughout the polymer matrix in all of the membranes.

Permeation experiments revealed that the addition of TiO<sub>2</sub> to the series 2 membrane increased the hydraulic permeability (Lp) from 13 to 50 kg/m<sup>2</sup>.bar relative to the CA reference membrane. In contrast, addition of TiO<sub>2</sub> to the membranes in series 1 did not increase the Lp in comparison to the CA/SiO<sub>2</sub> reference membrane. The Molecular Weight Cut-Off values were 9, 11, 5 and 10 kDa for the CA/SiO<sub>2</sub> (95:5 wt.%), CA/SiO<sub>2</sub>/TiO<sub>2</sub> (95:2:3 wt.%), CA (100 wt.%) and CA/TiO<sub>2</sub> (95:5 wt.%) membranes, respectively.

Further studies are needed to confirm the bactericide potential of the monophasic CA/SiO<sub>2</sub>/TiO<sub>2</sub> and CA/TiO<sub>2</sub> membranes against *Pseudomonas aeruginosa*. However, the two membranes from each series containing the highest TiO<sub>2</sub> content showed promising anti-biofouling properties as exopolysaccharide production was inhibited by CA/SiO<sub>2</sub>/TiO<sub>2</sub> (95:2:3 wt.%) and CA/TiO<sub>2</sub> (95:5 wt.%) membranes pre-treated with UV.

## Keywords:

Cellulose acetate membrane; Silica; Titania; Sol-gel; Monophasic material; Biofouling.

## 1 – Introduction

Cellulose acetate (CA) was one of the first polymers to be implemented in membranes by Loeb-Sourirajan in early 1960's [1]. Currently, CA membranes have a broad spectrum of flux profiles as reverse osmosis (RO) [2], nanofiltration (NF) [3], microfiltration (MF) [4] and ultrafiltration (UF) [5]. This versatility allows them to be used in different applications, including waste water treatment [3], gas separation [6], hemodialysis [7], bioprocess UF/NF separations [8], [9], etc. CA is an environmental friendly polymer and confers to the membrane great properties as flexibility, excellent water affinity, enhanced film-forming capacity, low footprint and cost [10]. Drawbacks that have been associated to CA membranes

are poor mechanical strength and thermal stability as well as susceptibility to biofouling [11].

Biofouling is one of the most serious problems in industrial applications and occurs due to the deposition, accumulation, growth and metabolism of microorganisms on membrane surface. It decreases membrane lifetime and fluxes and compromises the efficiency of the process. Some control strategies act on the elements affecting flux decline and can alleviate concentration polarization and membrane fouling. However, they are still expensive and difficult to optimize [12]. A novel approach for long-lasting biofouling control emerged with membrane functionalization with materials which have anti-adhesion and/or bactericide capacity, thus generating (hybrid) composite or monophasic membranes. Composite

membranes are biphasic systems based on weak interactions, which can compromise the membrane lifetime and efficiency due to poor phases adhesion [13]. Monophasic membranes only have one phase based on first order chemical bonds [14].

Mendes *et al.* [14] developed monophasic CA and silica (SiO<sub>2</sub>) (CA/SiO<sub>2</sub>) membranes. Hybrid monophasic CA/SiO<sub>2</sub> membranes were synthesized by promoting the in situ condensation between silanols from the SiO<sub>2</sub> precursor and the C–OH or acetate groups from the CA polymer. For all the CA/SiO<sub>2</sub> membranes, the ATR-FTIR peak assigned to (Si–O–C) proves the hybrid condensation reaction and confirms the synthesis of monophasic hybrid membranes. ATR-FTIR shows the presence of uncondensed highly reactive Si–OH species, in membranes with silica contents higher than 20 mol%. Together with RMN studies, results show molecular water strongly hydrogen-bonded with Si–OH groups, yielding a drastic decrease in the membrane hydraulic permeability, from 57 to 10 kg/h/m<sup>2</sup>/bar. The incorporation of 5 and 10 mol% of silica increased the hydraulic permeability from 32 to 82 kg/h/m<sup>2</sup>/bar when compared to the CA membrane.

Following the previous work, here is presented a preparation of monophasic CA/SiO<sub>2</sub>/TiO<sub>2</sub> membranes, using as starting material pure CA membrane and the CA/SiO<sub>2</sub> (95:5 wt.%) membrane.

Titania or titanium dioxide (TiO<sub>2</sub>) has been in the spotlight due to the discovery of its photocatalytic activity [15]. Recently, a distinction has been made between crystalline and amorphous TiO<sub>2</sub> (a-TiO<sub>2</sub>). The amorphous phase was believed to be photocatalytic inactive, however recently publications revealed the opposite [16], [17]. Some studies even hypothesize that the structure of a-TiO<sub>2</sub> promotes better/easy photocatalytic properties [18]. Recent research of Gonçalves *et al.* [18] developed nanoparticles (NPs) of a-TiO<sub>2</sub> for anti-microbial functions. The bactericide properties were determined in daylight and by incubating the NPs with *E. coli* ASTM E 2149 for 1h at room temperature. The results showed a 50% bactericide efficiency of NPs. In further experiments, the later were impregnated in cotton textiles [19]. The bactericide potential of the materials was studied in daylight for 24h at 35°C and against *S. aureus* ATCC®6538TM. The

bactericide efficiency of the impregnated cotton textiles varied from 16.93 to 99.97%. According to these researches, a-TiO<sub>2</sub> seems to be a promising material for membranes' functionalization and acquisition of anti-biofouling properties.

The present work aims to synthesize two series of novel monophasic CA/SiO<sub>2</sub>/TiO<sub>2</sub> (series 1) and CA/TiO<sub>2</sub> (series 2) membranes to improve both physical and anti-biofouling properties. The sol-gel method will be implemented to allow a co-condensation between SiO<sub>2</sub> and/or TiO<sub>2</sub> and CA polymer. The phase inversion technique will allow membranes' synthesis and conformation. This work membranes are chemically, morphologically and functionally characterized. In addition, the membranes are evaluated for permeation performance and rejection to solutes as well as for bactericide/anti-biofouling properties against, *Pseudomonas aeruginosa* (*P. aeruginosa*).

## 2 – Materials and Methods

### 2.1 – Material

The membranes were prepared with CA (C<sub>6</sub>H<sub>7</sub>O<sub>2</sub>(OH)<sub>3</sub>, ~30 000.00 g/mol, ≥97%, 40% of acetylation), tetraethylorthosilicate (TEOS) (Si(OC<sub>2</sub>H<sub>5</sub>)<sub>4</sub>, 208.33 g/mol, reagent grade 98%) and titanium(IV) isopropoxide (TIPO) (C<sub>12</sub>H<sub>28</sub>O<sub>4</sub>Ti, 284.00 g/mol, 97%), from Sigma-Aldrich (Overijse, Belgium), formamide (CH<sub>3</sub>NO, 45.02 g/mol, ≥99.5%) from Carlo Erba Reagents (Val-de-Reuil, France), acetone (C<sub>3</sub>H<sub>6</sub>O, 58.08 g/mol, 99.7%) and nitric acid (HNO<sub>3</sub>, 63.01 g/mol, >60%) from JMS (Odivelas, Portugal).

Membranes were dried by Solvent-Exchange with 2-propanol (C<sub>3</sub>H<sub>8</sub>O, 60.11 g/mol, ≥99.8% (GC)) from Honeywell (Maintal, Germany) and n-Henaxe (CH<sub>3</sub>(CH<sub>2</sub>)<sub>4</sub>CH<sub>3</sub>, 86.00 g/mol, ≥98.5% (GLC)) from Carlo Erba Reagents (Val-de-Reuil, France).

The hydraulic permeability tests were conducted with deionized water (H<sub>2</sub>O) and the solutes used for molecular weight cut-off (MWCO) were polyethylene glycols (PEGs) (HO(C<sub>2</sub>H<sub>4</sub>O)<sub>n</sub>H, 3, 4, 6, 10 and 20 kDa) from Merck (Darmstadt, Germany).

For bactericide/anti-biofouling tests the bacterial isolate used was *P. aeruginosa* C3719 [134].

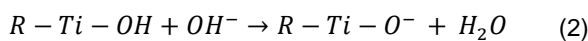
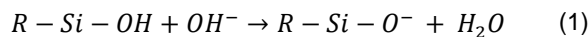
For protein quantification was used copper sulfate ( $\text{CuSO}_4$ , 249.68 g/mol) from Merck (Darmstadt, Germany) and for alginate quantification were used boric acid ( $\text{H}_3\text{BO}_3$ , 61.83 g/mol) from Merck (Darmstadt, Germany), sulfuric acid ( $\text{H}_2\text{SO}_4$ , 98.08, 95-97%) from Sigma-Aldrich (Overijse, Belgium) and carbazole ( $\text{C}_6\text{H}_4\cdot\text{NH}\cdot\text{C}_6\text{H}_4$ , 167.21 g/mol, 98%) from BDH Chemicals (Poole, UK).

## 2.2 – Membranes' synthesis

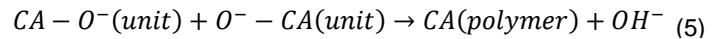
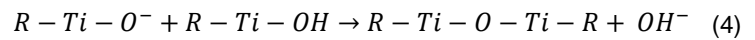
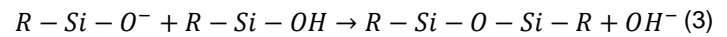
Membranes' casting solutions containing different concentrations of  $\text{SiO}_2$  and  $\text{TiO}_2$  were prepared by sol-gel [20] and phase inversion [5] techniques.

Series 1 components for the casting solution were added in the following order: CA, formamide, acetone, TEOS,  $\text{H}_2\text{O}$  and  $\text{HNO}_3$ . The flasks were sealed, and to obtain homogenous solutions were shaken for 24h in a magnetic stirrer. TIPOT ( $\text{TiO}_2$  precursor) was added to the casting solution, in a solution of acetone and formamide, after (due to faster hydrolysis rate). The casting solutions were prepared at room temperature, according to the compositions of **Table 1**. In series 2 the procedure was repeated, without the addition of TEOS ( $\text{SiO}_2$  precursor) (**Table 1**).

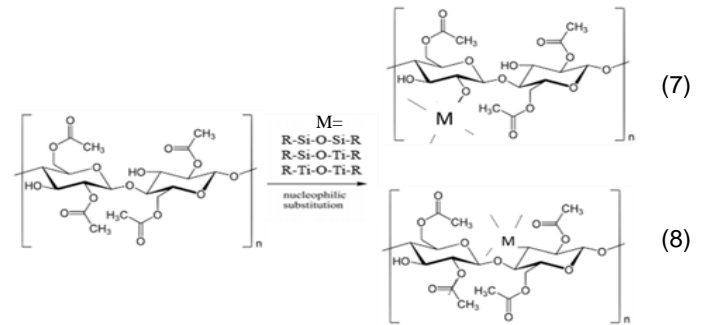
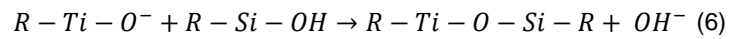
The sol-gel process takes place during the homogenization of the casting solution. In this process, hydrolysis and condensation reactions occur under acid catalysis:



After complete hydrolysis of  $\text{SiO}_2$  and  $\text{TiO}_2$  precursors, homo- and hetero-condensation reactions occur. Homo-condensations can be:



Hetero-condensations can be:



In **Eq. 7 and 8**, the M groups will perform a nucleophilic attack on the OH or  $\text{CH}_3\text{COOH}$  groups of CA. Forming in series 1, CA- $\text{SiO}_2$ - $\text{TiO}_2$  networks and in series 2, CA- $\text{TiO}_2$  networks.

The membranes' casting solutions were cast onto a glass plate at room temperature (19-23°C) with a 250  $\mu\text{m}$  casting knife, by the phase inversion method. After a solvent evaporation time of 30s the glass plates were immersed into a gelation bath. Following 1-2h of coagulation bath the membranes were stored in  $\text{H}_2\text{O}$  at approximately 4°C.

One batch of around 10 membranes was produce for each composition.

**Table 1 – Casting solution composition of series 1 and 2 membranes. The mass percentage of the components will be designated as: CA/ $\text{SiO}_2$ / $\text{TiO}_2$  (xCA:x $\text{SiO}_2$ :x $\text{TiO}_2$  wt.%).**

Casting solution (wt.%)	Series 1 (CA/ $\text{SiO}_2$ / $\text{TiO}_2$ )					Series 2 (CA/ $\text{TiO}_2$ )				
	(95:5:0 wt.%)	(95:4.5:0.5 wt.%)	(95:4:1 wt.%)	(95:3:2 wt.%)	(95:2:3 wt.%)	(100:0 wt.%)	(99.5:0.5 wt.%)	(98:2 wt.%)	(97:3 wt.%)	(95:5 wt.%)
CA	16.40	16.40	16.40	16.40	16.40	16.40	16.40	16.40	16.40	16.40
Formamide	29.00	29.00	29.00	29.00	29.00	29.00	29.00	29.00	29.00	29.00
Acetone	51.10	51.10	51.10	51.10	51.10	51.10	51.10	51.10	51.10	51.10
TEOS	3.00	2.70	2.40	2.10	0.93	0	0	0	0	0
TIPOT	0.00	0.32	0.64	0.96	2.07	0	0.32	0.96	2.07	3.00
$\text{H}_2\text{O}$	0.50	0.5	0.5	0.5	0.5	0.5	0.5	0.5	0.5	0.5
$\text{HNO}_3$	3 drops (pH ~ 1.5-2)									

## 2.3 – Morphology characterization

### 2.3.1 – Field Emission Gun–Scanning Electron Microscopy (FEG-SEM)

The membranes surface morphology and cross-section were characterized by FEG-SEM (JEOL 7001F JOEAL). Previously, the membranes were cut (1 cm<sup>2</sup> in the center) and dried by Solvent-Exchange adapted from [21]. Light elements energy-dispersive X-Ray spectroscopy (EDS) was used to evaluate TiO<sub>2</sub> precipitation on the membranes. Membranes' skin layer were measure in cross-section FEG-SEM images, with software ImageJ. For each composition, five distinct zones of the skin layer were measured, and the mean thickness and standard deviation was obtained.

### 2.3.2 – Inductively Coupled Plasma Optical Emission Spectrometry (ICP OES).

ICP OES was used to experimentally quantify: (i) the mass of titanium (Ti) in each membrane composition and (ii) the mass of Ti in a membrane lixiviation test.

In (i), 4 samples (2 squares of 16 cm<sup>2</sup> per membrane sheets) were taken for each composition. The samples were dried at room temperature until constant weight. To be analyzed by ICP OES the samples were dissolved. First, were placed in an Heraeus oven for 30 min at 550°C. After cooling, the ashes were solubilized in water and in acidic conditions (pH ≤ 2) with the help of a hotplate. The solution was injected in ICP OES (Optima 2000 of PerkinElmer) and atomized by the plasma. After excitation, metals decay emitting photons, which are detected and quantified. For comparison purposes the Ti mass in casting solution ( $m_{Ti}$ ) was calculated using:

$$m_{Ti} = \frac{W_m \times n_{TIPOT} \times MW_{Ti}}{M_T} \quad (9)$$

Where  $W_m$  is the total mass of the membrane sample weighed,  $n_{TIPOT}$  is the number of moles of TIPOT used in the casting solution (**Table 1**),  $MW_{Ti}$  is the molecular weight of Ti and  $M_T$  is the mass of a membrane sheet.  $M_T$  is obtained taking into account the masses of CA, TIPOT and TEOS used in the casting solution ( $M_T = M_{CA} + M_{TIPOT} + M_{TEOS}$ ). A homogeneous distribution of Ti throughout the membrane was assumed. The error propagation trough the calculations was obtained [22].

In (ii), only CA/SiO<sub>2</sub>/TiO<sub>2</sub> (95:2:3 wt.%) (series 1) and CA/TiO<sub>2</sub> (95:5 wt.%) (series 2) membranes were used. The assay was done in triplicate (with different membrane sheet samples). Ti leaching was studied by performing a permeation test with 500 mL of H<sub>2</sub>O<sub>d</sub> in Celfa-P28 [23]. The H<sub>2</sub>O<sub>d</sub> was recirculated for 3h at 0.6 L/min. The Ti content in final samples of H<sub>2</sub>O<sub>d</sub> collected in permeate and concentrate were analyzed by ICP OES.

### 2.3.3 – Attenuated Total Reflection–Fourier Transform Infra-Red (ATR-FTIR) spectroscopy

ATR-FTIR spectra of the top layer of all membrane were obtained and analyzed in Nicolet Magna IR System 5700 spectrometer (Nicolet Instrument Corp., Madison, USA), using a Golden Gate MKII ATR accessory with a Ge crystal (Graseby Specac, Smyrna; sampling depth: 0.2–1.1 μm at 4000–400 cm<sup>-1</sup>). Previous to observation, samples from of each membrane, were dried at room temperature. Each spectrum was obtained by averaging 256 scans with a resolution of 4 cm<sup>-1</sup>. The same number of background (clean ATR crystal) scans was taken. The spectra were transformed to log<sub>10</sub>(1/R) using the OMNIC software and are presented without baseline or smooth corrections.

The 1000-1110 cm<sup>-1</sup> ATR-FTIR bands of series 1 were decomposed by Gaussian curve-fitting (Levenberg Marquardt algorithm, allowing variation in width, height, and position of the bands), after a baseline correction (subtraction of a straight line between two extreme wavenumbers of the region). The number and starting position of the bands (used in the fitting) were obtained from the smoothed (Savitzky-Golay algorithm) second-derivative spectrum of the region. For each composition two individual peaks were found and a non-linear least-squares fitting procedure was performed to obtain 100% Gaussian shaped peaks. The quality of the fit was estimated through the evaluation of  $\chi^2$  remained constant. The ATR-FTIR spectra data was analyzed using Origin 8 pro software.

## 2.4 – Permeation capacity

Permeation tests were carried out in Celfa P-28 [23] with membrane area of 25 cm<sup>2</sup>. Before the experiments, the membranes were compacted with a pressure greater than

20% of the maximum working pressure, in recirculation mode and for 2-3h.

#### 2.4.1 – Hydraulic permeability

The membrane hydraulic permeability ( $L_p$ ) was obtained by the slope of the straight line of pure water permeate fluxes ( $J_p$ ) as a function of the  $J_p/\Delta P$  transmembrane pressure ( $\Delta P$ ) defined as  $=J_p/\Delta P$ . The  $L_p$  was estimated using two flow rates 0.6 L/min and 1.3 L/min and with a range of the transmembrane pressure of 0.5, 1, 1.5, 2, 2.5, 3 and 1, 1.5, 2, 2.5, 3, 3.5, respectively. Only one membrane sample per composition was analyzed.

#### 2.4.2 – MWCO determination

MWCO of the membranes was determined by the exclusion profile to PEG solutions with 600 ppm. The apparent rejection coefficient ( $f$ ) of each solute is calculated by  $f = \frac{C_b - C_p}{C_b}$ . Where  $C_b$  and  $C_p$  are the solute concentrations in the bulk feed solution and permeate solution, respectively. The solutes concentrations in feed and bulk solutions were determined in terms of total organic carbon in Shimadzu Total Organic Carbon Analyser TOC-V CSH. The MWCO is determined by  $\log(f/1-f)$  vs the molecular weights of the organic solutes and its intersection with the 90% rejection line, which correspond to  $\log(f/1-f)$  of 0.954. The assay was performed in CA/SiO<sub>2</sub> (95:5 wt.%), CA/SiO<sub>2</sub>/TiO<sub>2</sub> (95:2:3 wt.%), CA (100 wt.%) and CA/TiO<sub>2</sub> (95:5 wt.%) membranes. Only one membrane sample per composition was analyzed.

#### 2.5 – Bactericide/anti-biofouling properties

Three bactericide assays were performed, growth curve test, adhesion to membrane surface and cross-flow filtration of bacterial suspension. Prior to each assay, *P. aeruginosa* C3719 was grown in liquid LB broth overnight at 37°C and shaking at 250 rpm. This inoculum was then diluted, growth to exponential phase and used to initiate the experiments at an OD<sub>640nm</sub> of 0.1-0.4 equivalent to 10<sup>8</sup>/10<sup>9</sup> (CFU)/mL.

In growth curves, 9 mL of LB broth with and without the membranes were inoculated with 1 mL of inoculum. The

growth was followed at 30°C, 250 rpm for 30h based on OD measurements.

In adhesion to membrane surface, 1 mL of inoculum was filtered in the surface of the membranes. The membranes were incubated for 24h in LB plates at 30°C. After that, the number of cells grown in each membrane was counted by the CFU method.

In cross-flow filtration a suspension of *P. aeruginosa* cells (500 mL) was filtered at 30°C, 0.6L/min for 6h. The permeate flux along the filtration was followed. In the end, protein quantification by Biuret method [24] and alginate quantification [25] by carbazole method were performed in the membrane samples.

In all experiments, the membranes used were CA/SiO<sub>2</sub> (95:5 wt.%), CA/SiO<sub>2</sub>/TiO<sub>2</sub> (95:2:3 wt.%), CA (100 wt.%) and CA/TiO<sub>2</sub> (95:5 wt.%). The bactericide effect of CA/SiO<sub>2</sub>/TiO<sub>2</sub> and CA/TiO<sub>2</sub> membranes was evaluated with and without UV treatment for 1h.

### 3 – Results and discussion

#### 3.1 – Membranes' morphology

The SEM micrographs for CA/SiO<sub>2</sub> (95:5 wt.%) and CA/SiO<sub>2</sub>/TiO<sub>2</sub> (95:2:3 wt.%) membranes of series 1 and CA (100 wt.%) and CA/TiO<sub>2</sub> (95:5 wt.%) membranes of series 2 are shown in **Table 2**.

	Series 1	Top Layer	Cross-section	Bottom Layer
1	CA/SiO <sub>2</sub> (95:5 wt.%)			
1	CA/SiO <sub>2</sub> /TiO <sub>2</sub> (95:2:3 wt.%)			
	Series 2	Top Layer	Cross-section	Bottom Layer
	CA (100 wt.%)			
	CA/TiO <sub>2</sub> (95:5 wt.%)			

The top SEM images show a denser surface. Cross-section images show a skin denser layer on top outlining a thicker porous structure. The bottom SEM images show a porous surface. These features are characteristic of asymmetric membranes and are present in all compositions of the two series (data not shown). The presence of macro-voids was observed with TiO<sub>2</sub> introduction.

EDS analysis of the membranes' surface didn't show the presence of TiO<sub>2</sub> segregated phases (data not shown). The introduction of 0.5 and 1 wt.% of TiO<sub>2</sub> increase the thickness of the skin layer in series 1 membranes, comparative to the CA/SiO<sub>2</sub>. 2 and 3 wt.% of TiO<sub>2</sub> decreased the skin layer. In series 2, the skin layer thickness decreased for all membrane's comparative to the CA matrix (data not shown). A thin skin layer improves the permeation properties.

### 3.2 – Ti quantification

The mass of Ti introduced in the casting solution and the mass of Ti quantified on the membranes are in **Table 3**.

**Table 3 – Ti mass (mg) in the casting solutions and quantified in the membranes of series 1 and 2.**

Series 1	Ti in casting solution (mg)	Ti in membrane (mg)
CA/SiO <sub>2</sub> /TiO <sub>2</sub> (95:4.5:0.5 wt.%)	0.20±0.01	0.20±0.10
CA/SiO <sub>2</sub> /TiO <sub>2</sub> (95:4:1 wt.%)	0.44±0.01	0.40±0.10
CA/SiO <sub>2</sub> /TiO <sub>2</sub> (95:3:2 wt.%)	0.62±0.01	0.70±0.10
CA/SiO <sub>2</sub> /TiO <sub>2</sub> (95:2:3 wt.%)	1.28±0.01	1.20±0.20
Series 2	Ti in casting solution (mg)	Ti in membrane (mg)
CA/TiO <sub>2</sub> (99.5:0.5 wt.%)	0.31±0.01	0.50±0.10
CA/TiO <sub>2</sub> (98:2 wt.%)	0.76±0.01	1.30±0.30
CA/TiO <sub>2</sub> (97:3 wt.%)	1.66±0.01	1.30±0.50
CA/TiO <sub>2</sub> (95:5 wt.%)	2.39±0.01	2.00±0.20

For the two synthesized membrane series, the Ti mass introduced in the casting solution is similar to the mass quantified in the membrane's samples. Thus, an agreement between the casting solution and the final membrane composition was observed.

### 3.3 – Titania leaching

This assay aimed to assess if TiO<sub>2</sub> detaches from the membranes. **Table 4** shows the Ti concentration in H<sub>2</sub>Od

samples after filtration with the membranes. The initial and final samples of H<sub>2</sub>Od collected have the same Ti concentration. The result indicates that didn't occurred Ti leaching from the membranes which is an indicator of the covalent bond between TiO<sub>2</sub> and CA.

**Table 4 – Ti concentration (mg/L) in H<sub>2</sub>Od samples collected after filtration with CA/SiO<sub>2</sub>/TiO<sub>2</sub> (95:2:3 wt.%) (series 1) and CA/TiO<sub>2</sub> (95:5 wt.%) (series 2) membranes.**

Series 1	H <sub>2</sub> Od sample	[Ti] (mg/L)
CA/SiO <sub>2</sub> /TiO <sub>2</sub> (95:2:3 wt.%)	Initial	<0.010 ± 0.000
	Final permeate	<0.010 ± 0.000
	Final concentrate	<0.010 ± 0.000
Series 2	H <sub>2</sub> Od sample	[Ti] (mg/L)
CA/TiO <sub>2</sub> (95:5 wt.%)	Initial	<0.010 ± 0.000
	Final permeate	<0.010 ± 0.000
	Final concentrate	<0.010 ± 0.000

### 3.4 – TiO<sub>2</sub>–CA matrix molecular bonds

ATR-FTIR of series 1 and 2 was used to confirm the incorporation of SiO<sub>2</sub> and TiO<sub>2</sub> on the membranes. **Figure 1** shows the all spectra of series 1 and **Table 5** shows its complete band assignments.

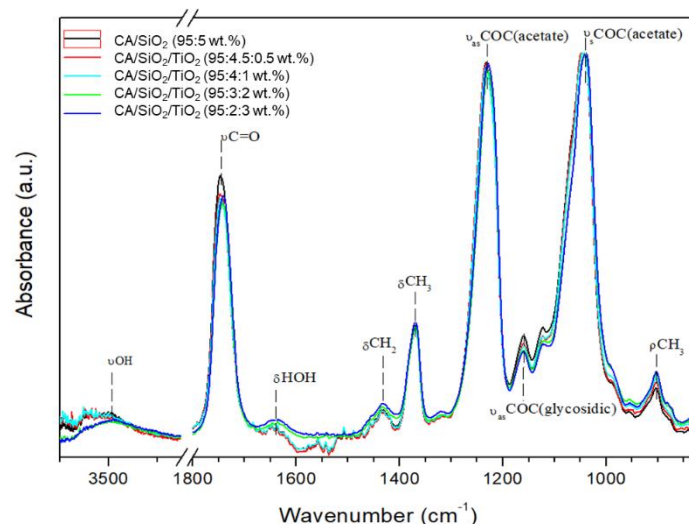


**Figure 1 – Complete ATR-FTIR spectra of series 1 membranes normalized to the C=O stretching band.**

The most intense bands for the series 1 membranes are found at: 1045 cm<sup>-1</sup> and 1232 cm<sup>-1</sup>, which correspond to the symmetric (νsCOC (acetate)) and antisymmetric (νasCOC

(acetate)) COC vibrations of the acetate group, respectively [26], [27]. Two characteristic bands of CA/SiO<sub>2</sub>,  $\nu(\text{Si-O-Si})$  and  $\nu(\text{Si-O-C})$  can also be found in this region, at 1065 cm<sup>-1</sup> and 1118 cm<sup>-1</sup> [14], respectively. Amplification of 1700-1800 cm<sup>-1</sup> strong band show that the addition of incremental amounts of TiO<sub>2</sub> decreases the carbonyl peak area and moves the band towards lower wavenumbers. This is a clear indication that TiO<sub>2</sub> preferred to bond to CA in the C=O group (data not shown). Amplification and decomposition in the region located between 1000 and 1110 cm<sup>-1</sup>, showed a peak shifting towards lower wavenumbers due to contribution Ti-O-C group ( $\nu\text{TiOC}$ ) (which absorbs in the region between 1039 and 1045 cm<sup>-1</sup>) [28], [29] (data not shown).

**Figure 2** shows the all spectra of series 2 and **Table 6** shows its complete band assignments. In ATR-FTIR spectra of series 2 the same intense bands of series 1 are observed. Amplification around 1700-1800 cm<sup>-1</sup> shows that addition of incremental amounts of TiO<sub>2</sub> results in an increase of the area of the carbonyl peak as well as its center moving to higher wavenumbers. The amount of CA in all of the membranes is equal in all membranes, so the increase of  $\nu\text{C=O}$  peak indicates that carbonyl groups are not being removed from the CA molecule for TiO<sub>2</sub> introduction (data not shown).

**Table 5 – Assignments of ATR-FTIR complete spectra for series 1 membranes.** VS - very strong; S -strong; m - medium; w - weak; vw - very weak; sh - shoulder; br – broad.

Wavenumber (cm <sup>-1</sup> )					Assignment
CA/SiO <sub>2</sub> (95:5 wt.%)	CA/SiO <sub>2</sub> /TiO <sub>2</sub> (95:4.5:0.5 wt.%)	CA/SiO <sub>2</sub> /TiO <sub>2</sub> (95:4:1 wt.%)	CA/SiO <sub>2</sub> /TiO <sub>2</sub> (95:3:2 wt.%)	CA/SiO <sub>2</sub> /TiO <sub>2</sub> (95:2:3 wt.%)	
3487 <sub>br</sub>	3490	3491	3489	3490	$\nu\text{OH}$ (H bonded)
1741 <sub>S</sub>	1742	1743	1736	1747	$\nu\text{C=O}$
1637 <sub>w</sub>	1637	1637	1637	1638	$\delta\text{HOH}$ (H <sub>2</sub> O)
1433 <sub>w</sub>	1432	1432	1431	1432	$\delta\text{CH}_2$
1369 <sub>m</sub>	1369	1369	1369	1369	$\delta_s\text{CH}_3$
1232 <sub>vs</sub>	1232	1232	1233	1232	$\nu_{as}\text{COC}$ (acetate)
1161 <sub>w</sub>	1161	1161	1161	1161	$\nu_{as}\text{COC}$ (glycosidic)
1122 <sub>w,sh</sub>	1122	1122	1122	1122	$\nu_{as}\text{COC}$ (glycosidic)
1065 <sub>w</sub>	1065	1065	1065	1065	$\nu_{as}\text{COC}$ (glycosidic), $\nu(\text{Si-O-Si})$
1045 <sub>vs</sub>	1045	1045	1045	1045	$\nu_s\text{COC}$ (acetate)
903 <sub>w</sub>	904	903	903	904	$\rho\text{CH}_3$

Amplification in 1000-1110 cm<sup>-1</sup> region shows a peak shift to higher wavenumber and a decrease in of area. The shift is probably due to the stretching vibration of the Ti-O-C group

( $\nu\text{TiOC}$ ) which absorbs at higher wavenumbers [28], [29] (data not shown).

The presence of Ti-O-C bonds evidences the establishment of covalent bonds between the inorganic (TiO<sub>2</sub>) organic (CA) components of the membranes in both series.

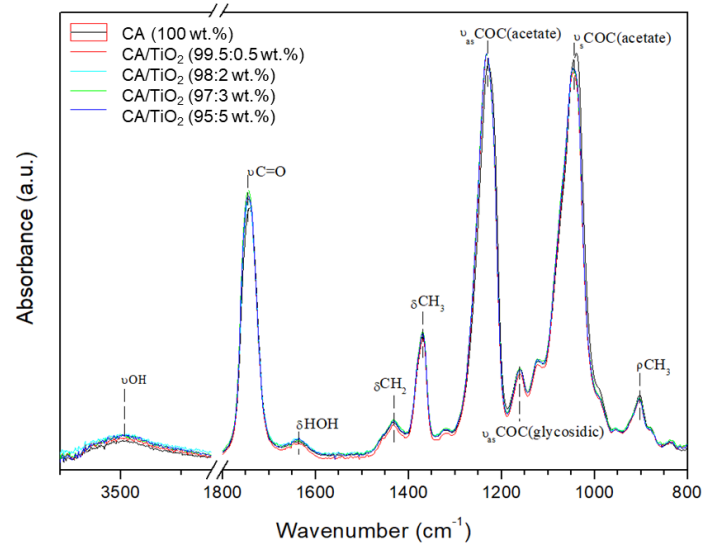


**Figure 2 – Complete ATR-FTIR spectra of series 2 membranes normalized to the C=O stretching band.**

**Table 6 – Assignments of ATR-FTIR complete spectra for series 2 membranes.** VS - very strong; S -strong; m - medium; w - weak; vw - very weak; sh - shoulder; br – broad.

Wavenumber (cm <sup>-1</sup> )					Assignment
CA (100 wt.%)	CA/TiO <sub>2</sub> (99.5:0.5 wt.%)	CA/TiO <sub>2</sub> (98:2 wt.%)	CA/TiO <sub>2</sub> (97:3 wt.%)	CA/TiO <sub>2</sub> (95:5 wt.%)	
3490 <sub>vs</sub>	3488	3494	3500	3500	$\nu\text{OH}$ (H bonded)
1739 <sub>S</sub>	1744	1745	1749	1749	$\nu\text{C=O}$
1635 <sub>w</sub>	1639	1636	1639	1639	$\delta\text{HOH}$ (H <sub>2</sub> O)
1435 <sub>w</sub>	1437	1430	1433	1433	$\delta\text{CH}_2$
1368 <sub>m</sub>	1379	1369	1379	1373	$\delta_s\text{CH}_3$
1233 <sub>vs</sub>	1234	1234	1234	1228	$\nu_{as}\text{COC}$ (acetate)
1165 <sub>w</sub>	1163	1163	1163	1163	$\nu_{as}\text{COC}$ (glycosidic)
1041 <sub>vs</sub>	1049	1045	1045	1045	$\nu_s\text{COC}$ (acetate)
898 <sub>w</sub>	903	903	897	903	$\rho\text{CH}_3$

### 3.5 – Hydraulic permeability

The Lp reveals the pure water permeation capacity of a membrane. **Figure 3** show the Lp values for each membrane composition of the two series.

In series 1, the incorporation of TiO<sub>2</sub> didn't enhance the Lp of the membranes relatively to the reference CA/SiO<sub>2</sub> (95:5 wt.%). In series 1 membrane probably occurred a pore size

reduction and low distribution. One possible justification is that the introduction of two inorganic counterparts interferes with the pore structure, resulting in more closed membranes that hinder the passage of solutes and the permeation performance.

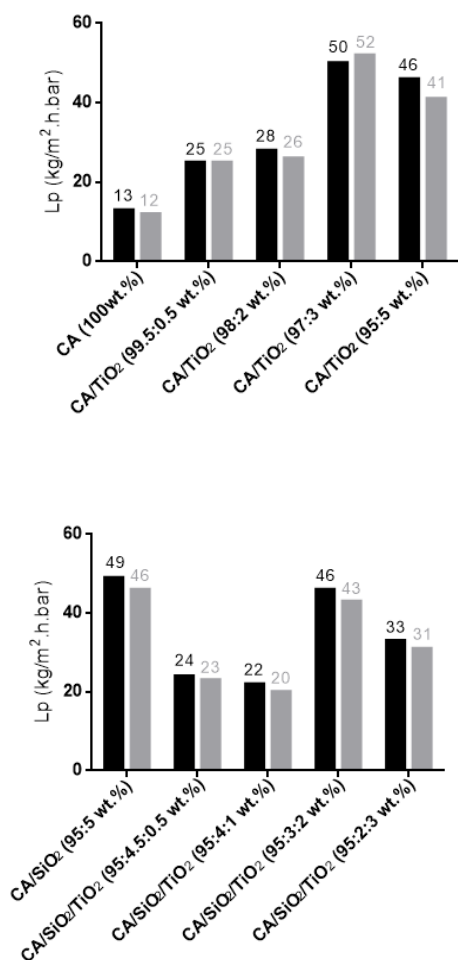


Figure 3 – Lp values for each membrane composition of series 1 (top) and series 2 (bottom).

In series 2, the TiO<sub>2</sub> increased the Lp of all membranes in comparison with the CA (100 wt.%) membrane.

The increase in mass percentage of TiO<sub>2</sub> increased the Lp, except for the CA/TiO<sub>2</sub> (95:5 wt.%) membrane. The later didn't follow the tendency, probably indicating a maximum of TiO<sub>2</sub> concentration from which the Lp starts to decrease.

### 3.6 – MWCO determination

The MWCO is the minimum molecular weight from which the membranes start to reject 90% of the solutes. The MWCO

for CA/SiO<sub>2</sub> (95:5 wt.%) and CA/SiO<sub>2</sub>/TiO<sub>2</sub> (95:2:3 wt.%) membranes of series 1 and CA (100 wt.%) and CA/TiO<sub>2</sub> (95:5 wt.%) membranes of series 2 are schematized in Table 7.

Series 1 membranes exhibited a MWCO of 9 kDa (CA/SiO<sub>2</sub> (95:5 wt.%) membrane) and 11 kDa (CA/SiO<sub>2</sub>/TiO<sub>2</sub> (95:2:3 wt.%) membrane). Series 2, MWCO of CA (100 wt.%) membrane was 5 kDa and of CA/TiO<sub>2</sub> (95:5 wt.%) membrane was 10 kDa. Both series are classified as ultrafiltration once its size exclusion is between 0.5 to 100 kDa [30].

Table 7 - MWCO values for CA/SiO<sub>2</sub> (95:5 wt.%) and CA/SiO<sub>2</sub>/TiO<sub>2</sub> (95:2:3 wt.%) membranes of series 1 and CA (100 wt.%) and CA/TiO<sub>2</sub> (95:5 wt.%) membranes series 2.

Series 1	MWCO (kDa)
CA/SiO <sub>2</sub> (95:5 wt.%)	9
CA/SiO <sub>2</sub> /TiO <sub>2</sub> (95:2:3 wt.%)	11
Series 2	MWCO (kDa)
CA (100 wt.%)	5
CA/TiO <sub>2</sub> (95:5 wt.%)	10

### 3.7 – Bactericide/anti-biofouling properties

*P. aeruginosa* (PA) growth curve with and without the membranes is shown in Figure 4. Growth parameters ( $\mu$  - specific growth rate (h<sup>-1</sup>) and tg - generation time) are shown in Table 8.

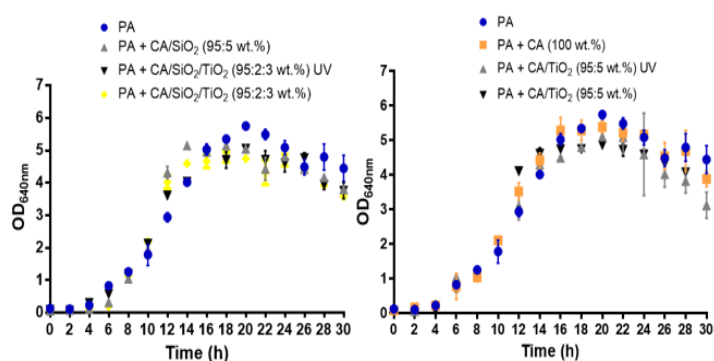


Figure 4 – Growth curves of *P. aeruginosa* with series 1 (left) and series 2 (right).

**Table 8 – Growth parameters and final biomass of the growth curves of Figure 4.**

Series	Sample	$\mu$ (h <sup>-1</sup> )	tg (h)	Final biomass (OD <sub>600nm</sub> )
1	PA	0.23±0.04	3.03±0.51	4.45±0.40
	PA + CA/SiO <sub>2</sub> (95:5 wt.%)	0.47±0.01	1.49±0.02	3.80±0.08
	PA + CA/SiO <sub>2</sub> /TiO <sub>2</sub> (95:2:3 wt.%) UV	0.32±0.02	2.19±0.11	3.76±0.25
2	PA + CA/SiO <sub>2</sub> /TiO <sub>2</sub> (95:2:3 wt.%)	0.48±0.02	1.46±0.07	3.58±0.08
	PA + CA (100 wt.%)	0.33±0.02	2.08±0.09	3.89±0.23
	PA + CA/TiO <sub>2</sub> (95:5 wt.%) UV	0.31±0.02	2.24±0.14	3.13±0.38
	PA + CA/TiO <sub>2</sub> (95:5 wt.%)	0.34±0.03	2.03±0.18	3.84±0.08

As seen in **Figure 4** the growth curves of *P. aeruginosa* with and without the membranes are very similar. The growth parameters are obtained by the exponential phase, where the cells are actively dividing. From **Table 8** is possible to observe that PA, *P. aeruginosa* growth alone (negative control), has a lower  $\mu$  than the other conditions. The membranes seem to stimulate the grow of the microbial cells. In series 1, the cells growth equally with CA/SiO<sub>2</sub> (95:5 wt.%) and CA/SiO<sub>2</sub>/TiO<sub>2</sub> (95:2:3 wt.%) and in series 2, with CA (100 wt.%) and CA/TiO<sub>2</sub> (95:5 wt.%). When the membranes are treated with UV the growth of the cells slows down slightly. At 30 h, the final biomass of cells is higher for PA without the membranes. The final biomass of cells with the membranes is similar. Once the growth is better with the membranes than the negative control, no loss of viability is suggested. At the end of growth, the lower biomass in growths with the hybrid monophasic membranes can be bactericide effect or cell adherence to the membranes. When the *P. aeruginosa* was grown in the surface of the membranes was shown that the *P. aeruginosa* show less 93% and 32% less CFU with the CA/SiO<sub>2</sub>/TiO<sub>2</sub> (95:2:3 wt.%) and CA/TiO<sub>2</sub> (95:5 wt.%) treated with UV light (data not shown).

**Figure 5** shows the permeate flux decay (%) during *P. aeruginosa* cell suspension filtration with the membranes and the initial and final fluxes.

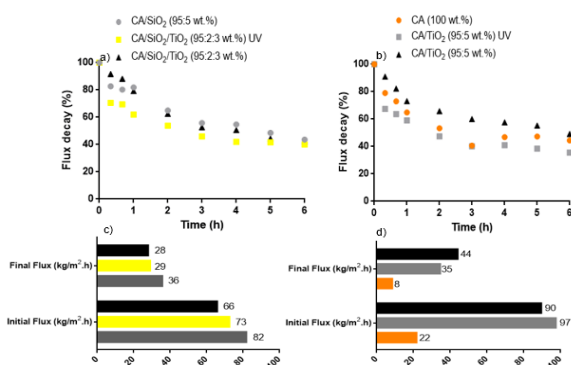


**Figure 5 – Flux decay (%) vs time (h) and initial and final permeate fluxes with: a and c) series 1 and b and d) series 2.**

The flux decay equally when filtering the *P. aeruginosa* cell suspension with series 1 and series 2 membranes. In series 1 membranes, introducing TiO<sub>2</sub> didn't improve the final flux after a filtration of a bacterial suspension. In series 2, CA/TiO<sub>2</sub> (95:5 wt.%) still present 450% higher flux than the CA (100 wt.%) membrane. Thus, despite the flux decreased equally with the two membranes, the CA/TiO<sub>2</sub> membrane still exhibits good permeation flux at the end. **Figure 6** shows the protein (viable bacterial cells) and alginate (exopolysaccharide) in the top surface of the membranes in the end of filtration.

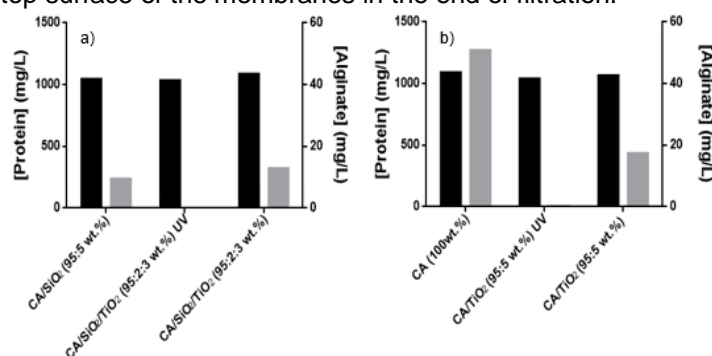


**Figure 6 – Protein and alginate concentration (mg/L) in the membrane surface of: a) series 1 and b) series 2.**

The protein represents the cells actively dividing in the membrane, which shows similar concentration through the membranes. Alginate is produced by *P. aeruginosa* during biofilm formation and is one of the causes of biofouling. The alginate concentration it's null when the CA/SiO<sub>2</sub>/TiO<sub>2</sub> (95:2:3 wt.%) and CA/TiO<sub>2</sub> (95:5 wt.%) membranes are treated with UV. The result suggest that the membranes have bactericide effect against *P. aeruginosa* leading to the loss of production of alginate. The results of protein concentration manifest possible bacteria contamination in the assay.

#### 4 – Conclusions

Two series of membranes, CA/SiO<sub>2</sub>/TiO<sub>2</sub> (series 1) and CA/TiO<sub>2</sub> (series 2) were prepared and characterized in terms of chemical structure, surface and cross-section morphology and permeation performance. The bactericide and anti-biofouling properties were evaluated using *P. aeruginosa*.

Surface and cross-section morphology studies demonstrated that the combination of sol-gel and phase inversion techniques was successful in the synthesis of integral skinned asymmetric membranes. According to FEG-

SEM images, increments of TiO<sub>2</sub> didn't affect the total thickness of the membrane but did have an influence on the dense skin layer thickness which is responsible for the resistance to mass transport imposed by the membrane. A thin skin dense layer improves membrane permeation performance and overall efficiency. Membrane characterization by ATR-FTIR and ICP OES revealed that, in the two series, TiO<sub>2</sub> is covalently bonded to CA and that the inorganic component is homogeneously distributed throughout the polymer matrix. ATR-FTIR spectra allow the confirmation of the proposed synthesis reactions shown in (Eq. 1-8).

Permeation experiments revealed that for the series 2 membranes Lp and MWCO increased with the increase of TiO<sub>2</sub>. The MWCO of the membranes from series 1 does not seem to be affected by TiO<sub>2</sub> content

Further studies are needed to confirm the bactericide potential of the CA/SiO<sub>2</sub>/TiO<sub>2</sub> and CA/TiO<sub>2</sub> membranes against *P. aeruginosa*. However, the two membranes from each series containing the highest TiO<sub>2</sub> content showed promising anti-biofouling properties.

Future work should include repletion of the experiments to evaluate bactericide effect of the membranes with controlled conditions to avoid contaminations, which may have influenced the final results. Furthermore, the anti-biofouling properties of membranes in longer-term filtration processes should be explored in order to access the membranes efficiency and lifetime in industrial applications.

## Acknowledgement

This document was written and made publicly available as an institutional academic requirement and as a part of the evaluation of the MSc thesis in Biotechnology of the author at Instituto Superior Técnico (IST). The work described herein was performed at ceFEMA and at IBB of IST (Lisbon, Portugal), during the period February-July 2019, under the supervision of Dr. Mónica Cristina Faria Besteiro and Prof. Maria Clara Henriques Baptista Gonçalves, as well as with the guidance of Prof. Isabel Maria de Sá-Correia Leite de Almeida.

## References

[1] S. and SRINIVASA and S. LOEB, "Sea Water Demineralization by Means of

- [2] an Osmotic Membrane," *In Saline Water Conversion—II*, pp. 117–132, 1963.
- [3] M. Sha *et al.*, "Cellulose acetate based thin film nanocomposite reverse osmosis membrane incorporated with TiO<sub>2</sub> nanoparticles for improved performance," *Carbohydr. Polym.*, vol. 186, pp. 367–376, 2018.
- [4] S. Beisl *et al.*, "Synthesis and bactericide activity of nanofiltration composite membranes – Cellulose acetate/silver nanoparticles and cellulose acetate/silver ion exchanged zeolites," *Water Res.*, pp. 225–231, 2019.
- [5] D. H. N. Perera *et al.*, "Room-temperature development of thin film composite reverse osmosis membranes from cellulose acetate with antibacterial properties," *J. Memb. Sci.*, vol. 453, pp. 212–220, Mar. 2014.
- [6] B. Kunst and S. Sourirajan, "An approach to the development of cellulose acetate ultrafiltration membranes," *J. Appl. Polym. Sci.*, vol. 18, no. 11, pp. 3423–3434, 1974.
- [7] J. Wu and Q. Yuan, "Gas permeability of a novel cellulose membrane," *J. Memb. Sci.*, vol. 204, pp. 185–194, 2002.
- [8] M. Sasaki *et al.*, "Vitamin E Modified Cellulose Membrane," *Artif. Organs*, vol. 24, pp. 779–789, 2000.
- [9] J. Qin *et al.*, "Cellulose acetate hollow fiber ultrafiltration membranes made from CA / PVP 360 K / NMP / water," *J. Memb. Sci.*, vol. 218, pp. 173–183, 2003.
- [10] J. Su *et al.*, "Cellulose acetate nanofiltration hollow fiber membranes for forward osmosis processes," *J. Memb. Sci.*, vol. 355, pp. 36–44, 2010.
- [11] B. S. Lalia *et al.*, "A review on membrane fabrication: Structure, properties and performance relationship," *Desalination*, vol. 326, pp. 77–95, 2013.
- [12] S. Vetrivel *et al.*, "Fabrication of cellulose acetate nanocomposite membranes using 2D layered nanomaterials for macromolecular separation," *Int. J. Biol. Macromol.*, vol. 107, pp. 1607–1612, 2018.
- [13] W. Zhang *et al.*, "A review on flux decline control strategies in pressure-driven membrane processes," *Ind. Eng. Chem. Res.*, vol. 54, no. 11, pp. 2843–2861, 2015.
- [14] J. Zhu *et al.*, "Polymeric antimicrobial membranes enabled by nanomaterials for water treatment," *J. Memb. Sci.*, vol. 550, pp. 173–197, 2018.
- [15] G. Mendes *et al.*, "Structure of water in hybrid cellulose acetate-silica ultrafiltration membranes and permeation properties," *Carbohydr. Polym.*, vol. 189, pp. 342–351, 2018.
- [16] A. FUJISHIMA and K. HONDA, "Electrochemical Photolysis of Water at a Semiconductor Electrode," *Nature*, vol. 238, pp. 37–38, 1972.
- [17] Y. Li *et al.*, "Hexagonal-close-packed, hierarchical amorphous TiO<sub>2</sub> nanocolumn arrays: Transferability, enhanced photocatalytic activity, and superamphiphilicity without UV irradiation," *J. Am. Chem. Soc.*, vol. 130, no. 44, pp. 14755–14762, 2008.
- [18] C. Randorn *et al.*, "Synthesis of visible-light-activated yellow amorphous TiO<sub>2</sub> photocatalyst," *Int. J. Photoenergy*, pp. 1–6, 2008.
- [19] M. C. Gonçalves *et al.*, "Photonic Band Gap and Bactericide Performance of Amorphous Sol-Gel Titania: An Alternative to Crystalline TiO<sub>2</sub>," *Molecules*, vol. 23, p. 1677, 2018.
- [20] J. C. Matos *et al.*, "Daylight bactericidal titania textiles: A contribution to nosocomial infections control," *Molecules*, vol. 24, no. 1891, pp. 1–15, 2019.
- [21] J. Brinker and G. Scherer, "Sol-gel science: The physics and chemistry of sol-gel processing presents the physical and chemical principles of the sol-gel process," *Gulf Prof. Publ.*, 1990.
- [22] A. Lui *et al.*, "Studies on the solvent exchange technique for making dry cellulose acetate membranes for the separation of gaseous mixtures," *J. Appl. Polym. Sci.*, vol. 36, no. 8, pp. 1809–1820, 1988.
- [23] S. J. Kline and F. A. McClintock, "Describing uncertainties in single-sample experiments," *Mech. Eng.*, vol. 75, no. 1, pp. 1–8, 1953.
- [24] M. A. R. Sousa, "Clarificação e estabilização proteica de vinhos por Ultrafiltração," 2017.
- [25] D. Herbert, P. J. Phipps, and R. E. Strange, *Chapter III Chemical Analysis of Microbial Cells*. 1971.
- [26] A. C. Knutson and A. Jeanes, "A New Modification of Carbazole Analysis: Application to Heteropolysaccharides," *Anal. Biochem.*, vol. 24, pp. 470–481, 1968.
- [27] D. Murphy and M. N. de Pinho, "An ATR-FTIR study of water in cellulose acetate membranes prepared by phase inversion," *J. Memb. Sci.*, vol. 106, pp. 245–257, 1995.
- [28] A. Ahmad *et al.*, "Effect of silica on the properties of cellulose acetate/polyethylene glycol membranes for reverse osmosis," *Desalination*, vol. 355, pp. 1–10, 2015.
- [29] M. T. Harris *et al.*, "FTIR Spectroscopy, SAXS and Electrical Conductivity Studies of the Hydrolysis and Condensation of Zirconium and Titanium Alkoxides," *J. Sol-Gel Sci. Technol.*, vol. 8, no. 1–3, pp. 41–47, 1997.
- [30] M. J. Velasco *et al.*, "Hydrolysis Of Titanium Tetrabutoxide. Study by FT-IR Spectroscopy," *Spectrosc. Lett.*, vol. 32, no. 2, pp. 289–304, 1999.
- [31] Z. F. Cui *et al.*, *Fundamentals of Pressure-Driven Membrane Separation Processes*, First Edit. Elsevier Ltd, 2010.